Proceedings World Geothermal Congress 2020+1
Reykjavik, Iceland, April - October 2021

Application of Digital Image Processing Techniques of Earth Observation Satellites in the Estimation of Surface Temperature Models in Support of Geothermal Exploration in Colombia

J. Camilo Matiz-León, Gilbert Rodríguez-Rodríguez and Claudia Alfaro-Valero

Colombian Geological Survey – SGC

Diagonal 53 No. 34-53 Bogotá D.C., Colombia

jmatiz@sgc.gov.co

Keywords: geothermal exploration, shallow surface temperature, remote sensing, NDVI, digital satellite image processing, geostatistics, Pearson.

ABSTRACT

The obtaining of models of surface temperature by means of Shallow Temperature Surveys (SST), shows a first approach to surface temperature anomalies in the exploration stage of a geothermal area of interest in a fast, portable and economic way. In the Colombian Geological Survey (SGC), the SST materializes at depths between 20 cm and 150 cm, taking into account the normalization of data to eliminate the influence of solar radiation, thermal diffusion, albedo, slopes, relief, and the effect of climatic seasons. As a method parallel to the estimation of temperature models of the terrestrial surface, the Remote Sensing (RS) are integrated that have satellite images of terrestrial observation in the thermal infrared. Based on the ground truth established by the SST, the degree of positive or negative correlation is estimated with the temperature models estimated by RS, reaching a method of validation between remote sensing techniques and the ground truth. Within the proposed methodology, the processing of a temperature model from RS images is proposed, specifically the image processing with bands in the thermal infrared (like Landsat 8 TIRS) of the geothermal area. The validation of the model achieved through the Digital Image Processing (PDI), is performed against the ground truth (SST) through qualitative and quantitative analysis with variables such as vegetation indices or anomalies of radioactive elements such as Uranium (^{38}U), Thorium (^{32}Th) and Potassium (^{40}K) by gamma-ray spectrometry, according to the availability of information in each geothermal area. In order to establish a positive or negative correlation between the temperature anomalies estimated from different techniques (SST vs RS), parametric correlation tests were performed pixel by pixel (Pearson coefficient).

1. INTRODUCTION

One of the sources of thermal data associated with the Earth's surface is derived from Earth observation satellites placed in orbit. These sensors allow capturing radiance values in the near infrared, included in the digital number (DN) of the pixel that by means of PDI can express values in units of temperature (Mwawongo, 2007). As the image taking suggests that the wavelength is affected by the interference of solar radiance, vegetation and climate, a series of corrections are applied to the DN to calculate the temperature values and vegetation indices that adjust to the geothermal reality (Abouriche, 1989). To validate these models derived from the RS as ground truth have the SST for the characterization of temperature anomalies near the earth's surface (Mwawongo, 2007).

Because the cost-benefit evaluation in the exploration stage takes a lot of relevance in the interpretation of the temperature anomalies present in the geothermal systems (Olmsted & Ingebritsen, 1986), the contribution in the characterization of temperature anomalies from models extracted by RS, lies in the contribution of this input in the pre-feasibility stage of the study area for decision-making aimed at identifying the elements and components of the geothermal area (Coolbaugh et al., 2014). This contribution is essential, since generally, the exploration phase in the nonexistent geothermal industry in the Colombian territory, consumes many financial resources dedicated to the identification of the elements of the conceptual model to evaluate the energy potential (Olmsted and Ingebritsen, 1986; Kratt et al 2009; Beardsmore, 2012; Matiz-León, 2015).

2. METHODOLOGY

The research methodology corresponds to the processing of a temperature model from RS images, specifically the processing of Landsat 8 TIRS images (bands 10 and 11) of the geothermal area. In turn, the calculation of vegetation indices is included, generated with the bands of visible red and near-infrared (NIR) (Becerra-González et al., 2016) of Landsat 8 OLI images (bands 4 and 5), which allows to identify spatially the density and type of living vegetation, in order to corroborate the spatial variations of the surface temperature with the presence of vegetation (Norini et al., 2015). The validation of the model achieved through the PDI was made against the ground truth constructed through the SST by means of the qualitative analysis of the treatments generated for each image. In order to establish a quantitative measure of the relationship between the variables (temperature calculated by the SST and RS), parametric correlation tests (Pearson) was performed due to the normality of the data (Baddi et al., 2014).

2.1 Materials

2.1.1 Landsat 8 TIRS and OLI

The processed images are downloaded under criteria such as shooting dates close to the dates of SST drilling and cloudiness less than or equal to 10 % in each scene (Kratt et al., 2009). From these images the thermal bands 10 and 11 of the Thermal InfraRed Sensor (TIRS) were used with wavelengths of 10,60 µm – 11,19 µm and 11,50 µm – 12,51 µm, respectively, with a spatial resolution of 100 m, redistributed at 30 m and the red and near-infrared bands of the Operational sensor Land Imager (OLI) (wavelength between 0,64 µm to 0,88 µm with spatial resolution of 30 m) (USGS, 2016).

2.1.2 Digital Elevation Model – DEM

The heights of the study area are based on the Digital Elevation Model - MDE of the National Aeronautics and Space Administration (NASA) and the National Geospatial-Intelligence Agency (NGA), known as the Shuttle Radar Topography Mission (SRTM) with an overall accuracy of 1 second of arc or in reference systems projected at 30 m (Farr et al., 2007). The SRTM uses the C band of the Aerospace Radar Imaging platform and the X band of the Synthetic Aperture Radar (X-SAR).

2.1 Methods

2.2.1 Surface Temperatures

The surface temperatures are calculated from the data taken in the field by drilling the boreholes to the depths of 20 cm, 100 cm, and 150 cm with a separation distance between soundings of 1 km (Coolbaugh et al., 2007; Rodríguez, 2016). For the representation of the temperatures, a statistical analysis was generated for each of the data sets at different recorded depths, composed of Quantile - Quantile diagrams $(Q - Q)$, semivariograms and the review of the global data trend (Rodríguez, 2016).

$$T_s^\circ = 28{,}1 - 0.00553 * h \tag{1}$$

The calculation of the surface temperature was based on (1), where T_s° corresponds to the annual average air temperature in $°C$ and h to the altitude in meters (Eslava, 1992). This equation was developed from the taking of values of meteorological stations located in the colombian territory during different dates. The time interval corresponded to 10 years during which the values were collected (Eslava, 1992).

2.1.2 Temperatures normalization with reference to T_s°

Once calculated the T_s° temperature data are normalized by measured depth, taking into account that temperature surveys were measured at different times and daily variation of the solar rays affects each of the recorded values (Rodríguez, 2013). This normalization with the purpose of eliminating the effect of the sun in each one of the surveys is based on the difference of the temperatures found in depth and the T_s° (equation 2).

$$T_{norm}^\circ = T_{prof}^\circ - T_s^\circ \tag{2}$$

Where T_{norm}° is the normalized temperature and T_{prof}°, the temperature measured in depth. This standardization is applied for each of the depths reached (Rodríguez, 2013). This form of standardization was applied to measurements made at 20 cm, 100 cm and 150 cm, taking into account that these depths are quite shallow and the incidence of solar radiation in the subsoil is still inferred. The values obtained correspond to the variation of the temperature on a scale of centimeters.

2.1.3 Geostatistics

The Kriging Simple method was applied, using the theoretical model of the Gaussian variogram, a lag (h) of up to 1000 m distance and a neighborhood parameter corresponding to the number of neighbors involved in spatial interpolation (15 surveys) (Rodríguez, 2016). In Figure 1 and Figure 2, interpolations are represented for temperatures reached at 150 cm depth for Azufral Volcano and Paipa Geothermal areas respectively.

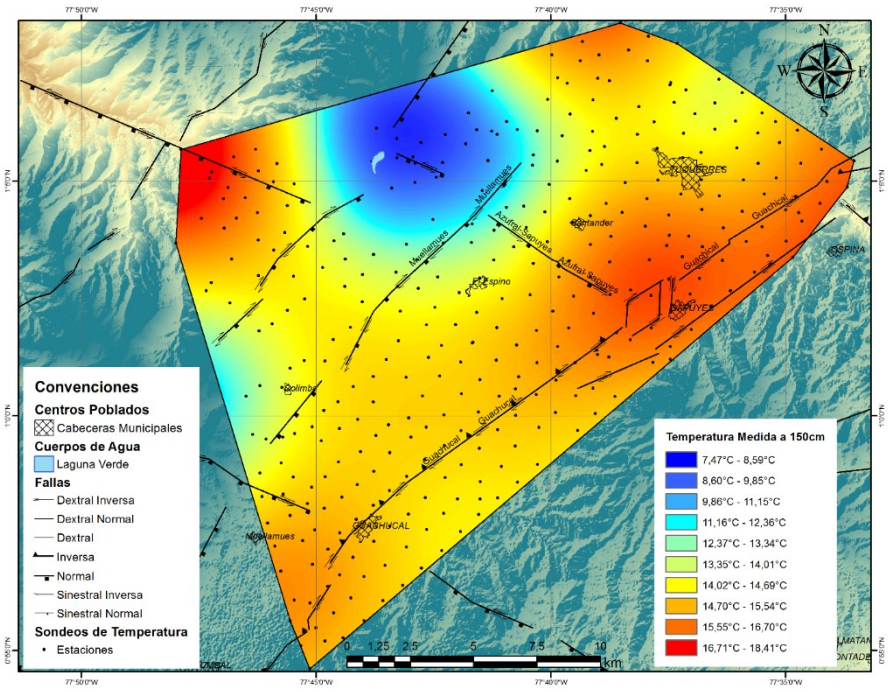

Figure 1: Interpolated temperatures with geostatistics at 150 cm depth for Azufral Volcano geothermal area.

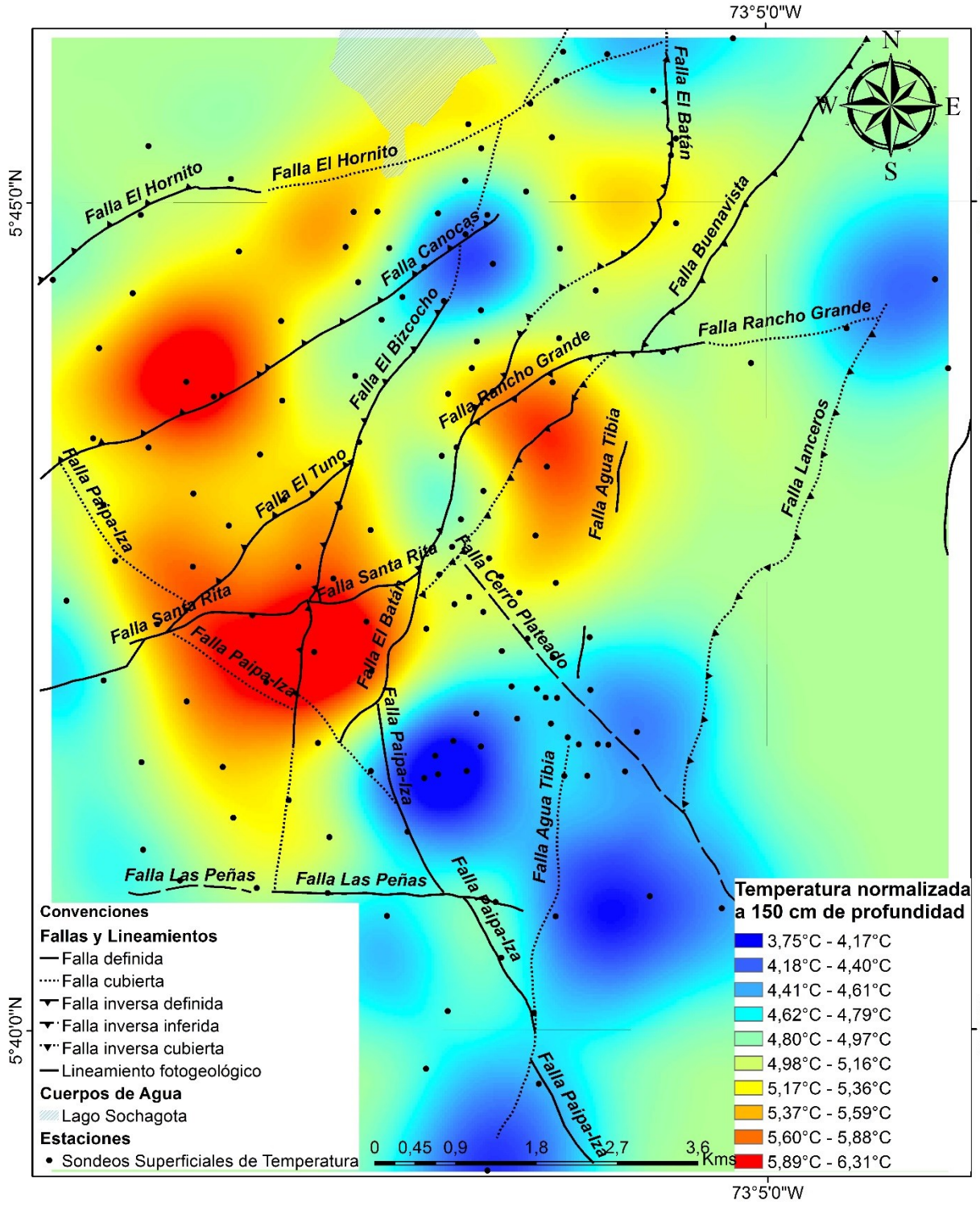

Figure 2: Interpolated temperatures with geostatistics at 150 cm depth for Paipa geothermal area.

2.1.4 Surface temperatures from Digital Number

The calculation of the temperatures from the Landsat 8 images, consists of the transformation of the Digital Numbers (DN) to radiance values by means of (3) (USGS, 2016).

$$radiancia_{multibanda_x} * banda_{termica_x} + radiancia_{add\_banda_x} \quad (3)$$

In the metadata image there are the respective radiometric reescalation coefficients: $radiancia_{multibanda_x}$ corresponds to the multiplicative adjustment factor of the radiance in each band, $banda_{termica_x}$ corresponds to the thermal band of the TIRS sensor to be used and $radiancia_{add\_banda_x}$ corresponds to the additive adjustment factor of the radiance in each band used (USGS, 2016). This procedure can be applied in (3) and (4) for bands 10 and 11 of the TIRS sensor (Li et al, 2005). Subsequently the radiance is transformed into apparent brightness temperature values T_{Kelvin} (equation 4).

$$T_{Kelvin} = \frac{K2}{\ln\left(\frac{K1}{L\lambda}+1\right)} \quad (4) \qquad T_{Celsius} = T_{Kelvin} - 273.15 \quad (5)$$

Where $K1$ and $K2$ correspond to the thermal conversion constants for each band of the image and $L\lambda$ is the reflectance in the upper part of the atmosphere Top of Atmosphere (TOP) (USGS, 2016). The calculated temperature is represented in degrees Kelvin, so it is transformed to degrees Celsius (equation 5) (USGS, 2016). This procedure can be applied for bands 10 and 11 of the TIRS sensor (Li et al, 2005). In Figure 3 and Figure 4, the temperatures calculated from the Landsat 8 TIRS sensor images are shown for Paipa and Azufral Volcano geothermal area respectively.

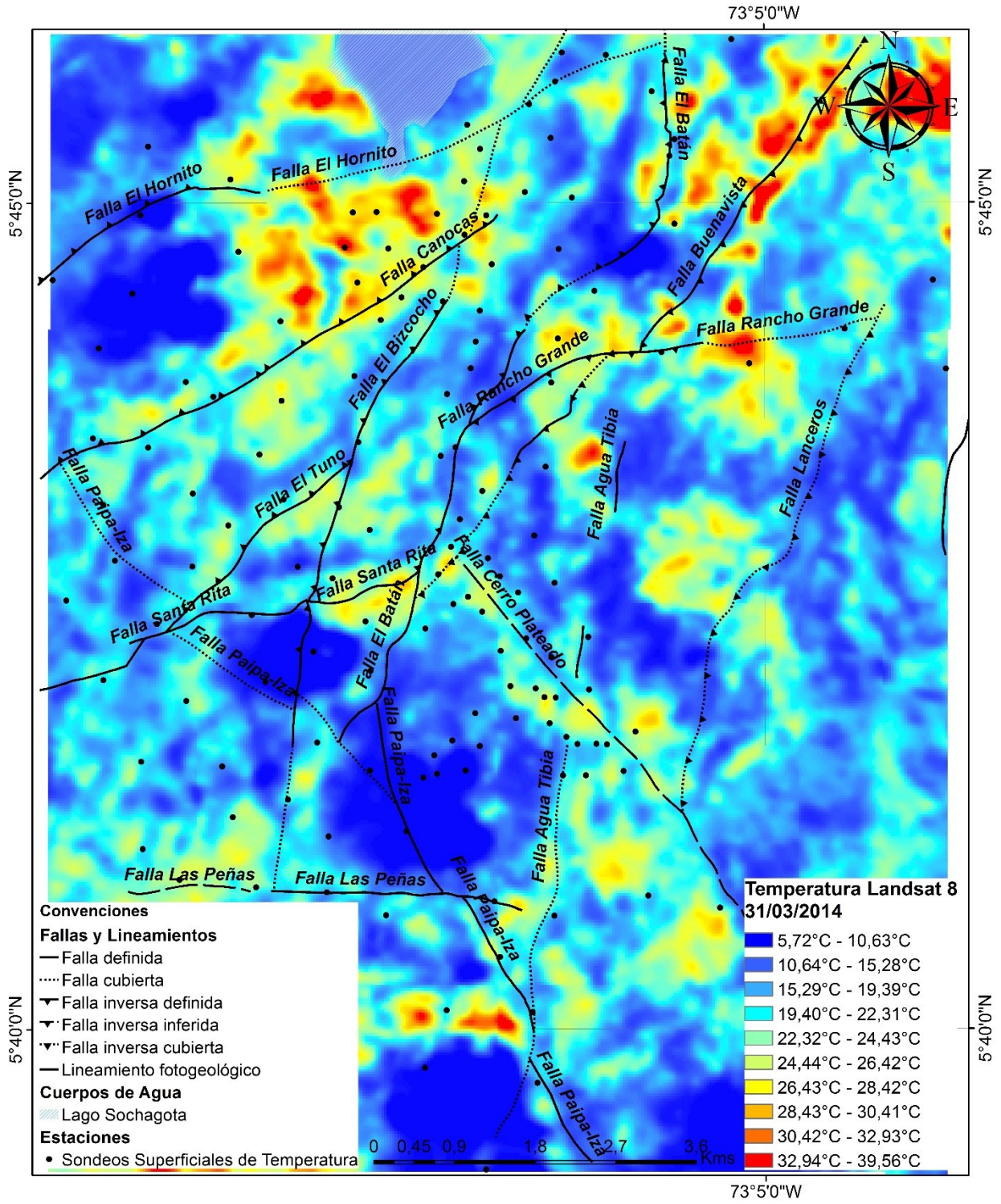

Figure 3: Temperatures calculated with Landsat 8 TIRS thermal bands for Paipa geothermal area.

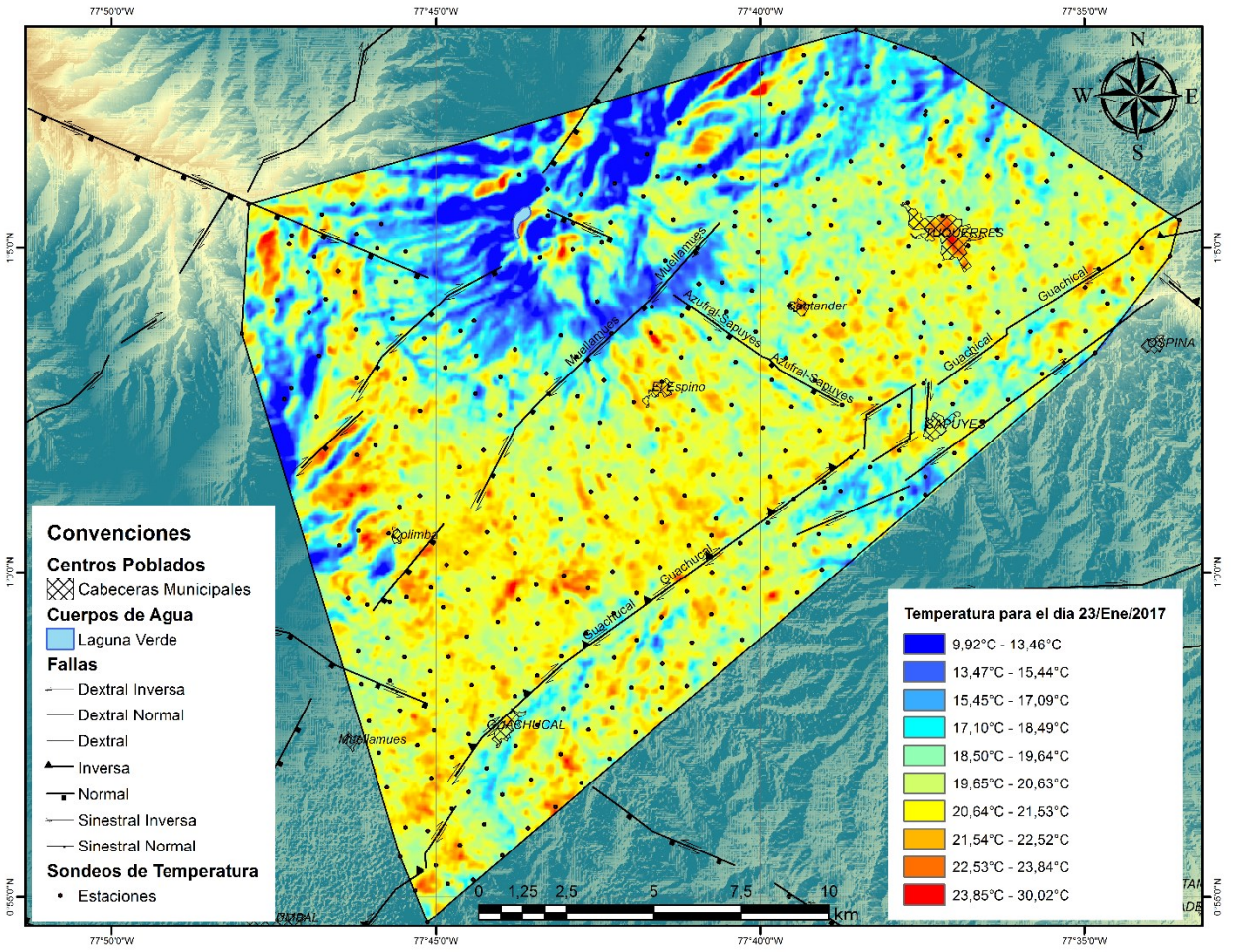

Figure 4: Temperatures calculated with Landsat 8 TIRS thermal bands for Azufral Volcano geothermal area.

2.1.5 Temperature normalization with reference to the RS surface temperature

To compare the temperature differences in depth by eliminating the effect of the sun, the normalization applied to temperature values calculated from the Landsat thermal bands was applied, based on the surface temperature calculated with TIRS images and make de difference with Landsat temperature $T^{\circ}_{Sup\_Landsat}$.

2.1.6 Vegetation Indexes

In the estimation of the Normalized Differential Vegetation Index (NDVI), the values to measure the vegetation in the NDVI range from -1 to +1, where the values higher or close to 1 represent a vegetative cover with greater greenness (mostly healthy and free of stress) (Mermer, 2015). In the equation, the reflectance DN of visible red and NIR were transformed into indices for each pixel, through (6) (Mermer, 2015). In Figure 5, the result achieved for a geothermal area in exploration is observed.

$$NDVI = \frac{NIR-Rojo}{NIR+Rojo} \tag{6}$$

3. VALIDATION

3.1 Correlation between variables: pixel to pixel - Pearson coefficient

A correlation coefficient measures the degree of relationship between two random variables (Restrepo and González, 2007). The Pearson coefficient measures the degree of association between quantitative random variables with normal distribution bivariate joint (Baddi et al., 2014). For the correlation analysis between the same temperature variable from two different sources of information (ground truth = SST and hypothesis = RS), the correlation was made pixel by pixel, by transforming each image (interpolated and processed) as a matrix array and treated under the processing of statistical software

$$\rho_{X,Y} = \frac{\sigma_{XY}}{\sigma_X \sigma_Y}, where -1 \leq \rho_{X,Y} \leq 1 \tag{7}$$

Where, $\rho_{X,Y}$ is the Pearson correlation coefficient, σ_{XY} the covariance of the variables XY, σ_X the standard deviation of the variable X and σ_Y the standard deviation of the variable Y (Restrepo and González, 2007). Table 1 shows the coefficients obtained from the pixel to pixel correlation.

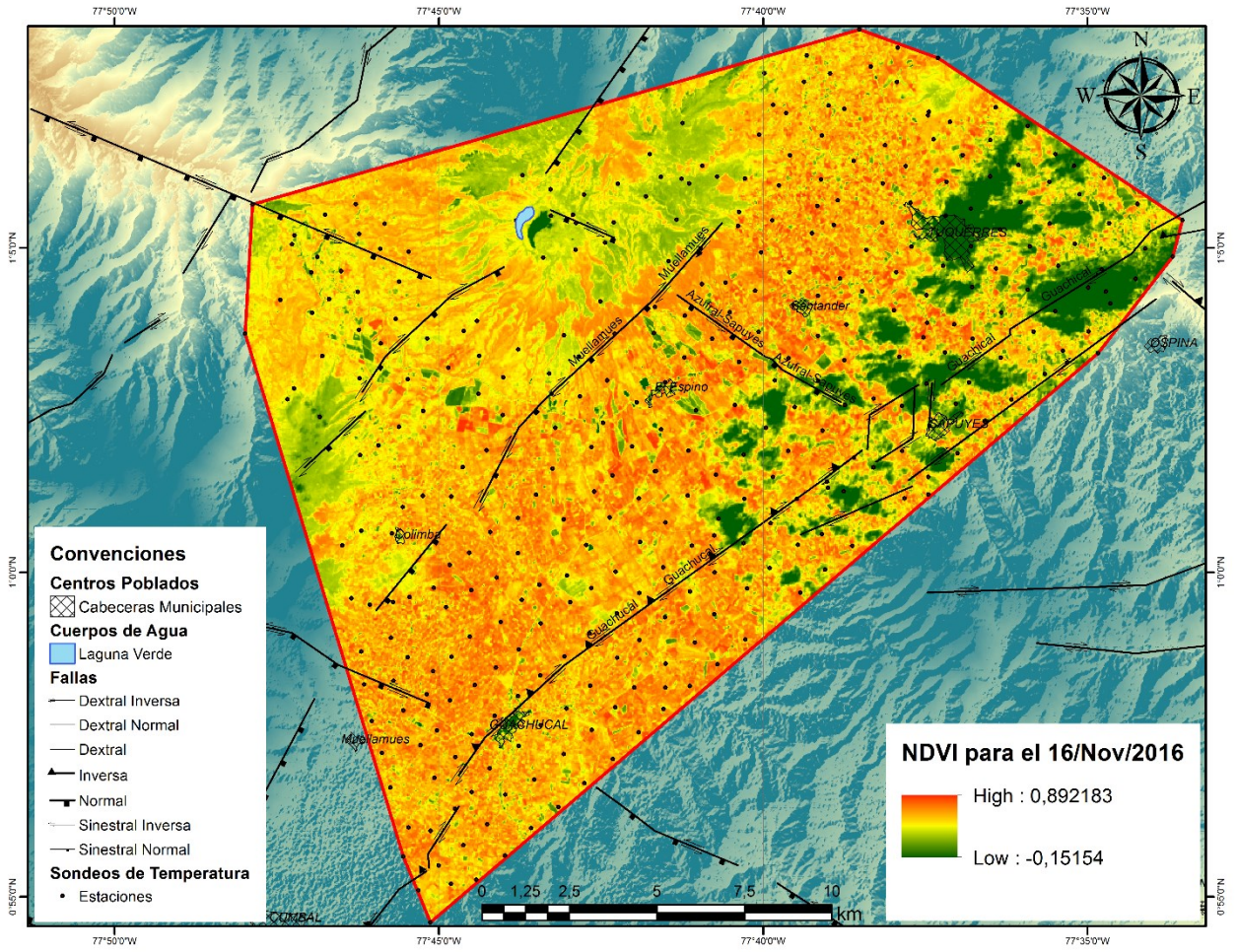

Figure 5: Normal Differentiated Vegetation Index - NDVI with Landsat 8 OLI red and near infrared bands.

Table 1: Example of Pearson correlation coefficients for RS surface temperatures.

Variables	Pearson coefficient
Temperature calculated based on height vs. temperature calculated by RS for 15/Sep/2015	0,2104
Temperature calculated based on height vs. temperature calculated by RS for 20/Nov/2016	0,1928
Temperature calculated based on height vs. temperature calculated by RS for 23/Jan/2017	0,4388

Variables	Pearson coefficient
Temperature measured in surface vs temperature calculated by RS for 15/Sep/2015	0,2746
Temperature measured in surface vs temperature calculated by RS for 20/Nov/2016	0,0547
Temperature measured in surface vs temperature calculated by RS for 23/Jan/2017	0,3627

3.2 Cross sections analysis

To compare the positive and negative anomalies and the respective correlation between variables, cross sections are drawn, covering the areas of interest in the work area, which allow to identify the variations along the profile of the topography (height above sea level), the temperature according to the depth of measurement, the day of capture of the sensor and the vegetation indexes and variables that enrich the interpretation and of which data are available, such as Uranium (^{38}U), Thorium (^{32}Th) and Potassium (^{40}K) (González et al., 2008).. In Figure 6 shows the interpolation for Uranium, Thorium and Potassium respectively.

a)

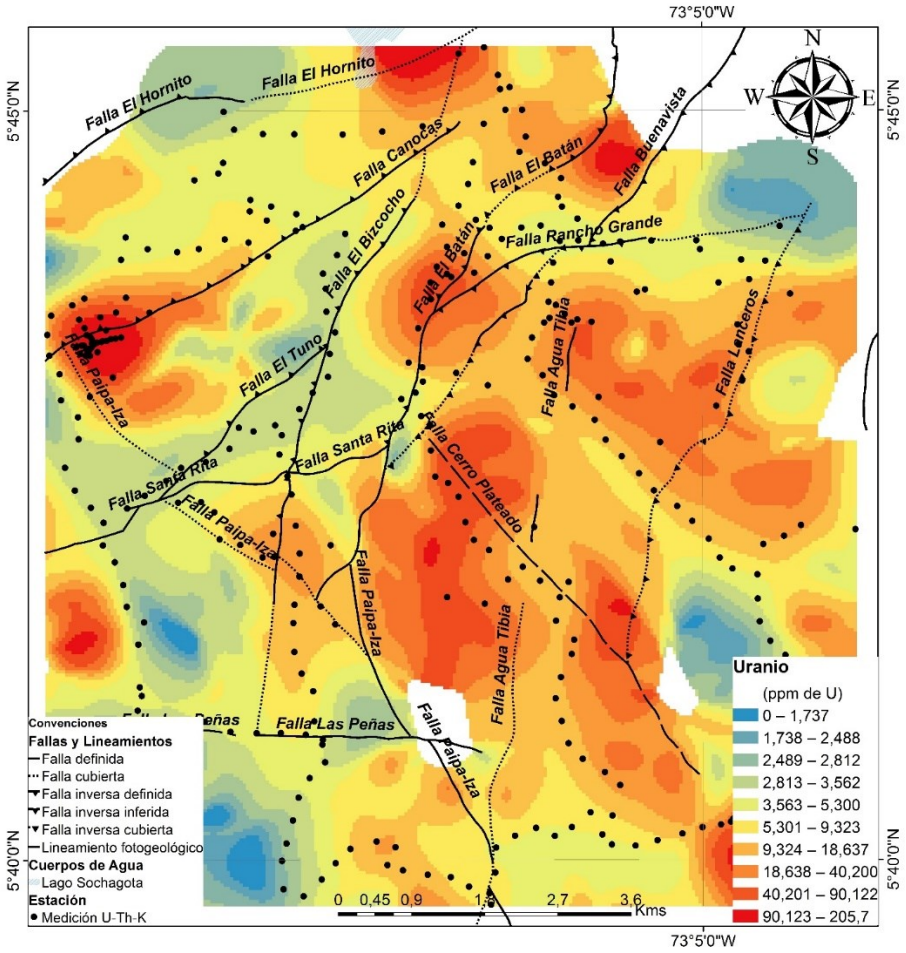
73°5'0"W
5°45'0"N
5°40'0"N
N
W
E
S
Falla El Hornito
Falla Canoas
Falla El Batán
Falla Buenavista
Falla Rancho Grande
Falla El Bizcocho
Falla Agua Tibia
Falla Lenteros
Falla El Tuno
Falla Paipa-Iza
Falla Santa Rita
Falla Cerro Plateado
Falla Las Peñas
Convenciones
Fallas y Lineamientos
Falla definida
Falla cubierta
Falla inversa definida
Falla inversa inferida
Falla inversa cubierta
Lineamiento fotogeológico
Cuerpos de Agua
Lago Sochagota
Estación
Medición U-Th-K
0 0,45 0,9 1,8 2,7 3,6 Kms
Uranio
(ppm de U)
0 – 1,737
1,738 – 2,488
2,489 – 2,812
2,813 – 3,562
3,563 – 5,300
5,301 – 9,323
9,324 – 18,637
18,638 – 40,200
40,201 – 90,122
90,123 – 205,7

b)

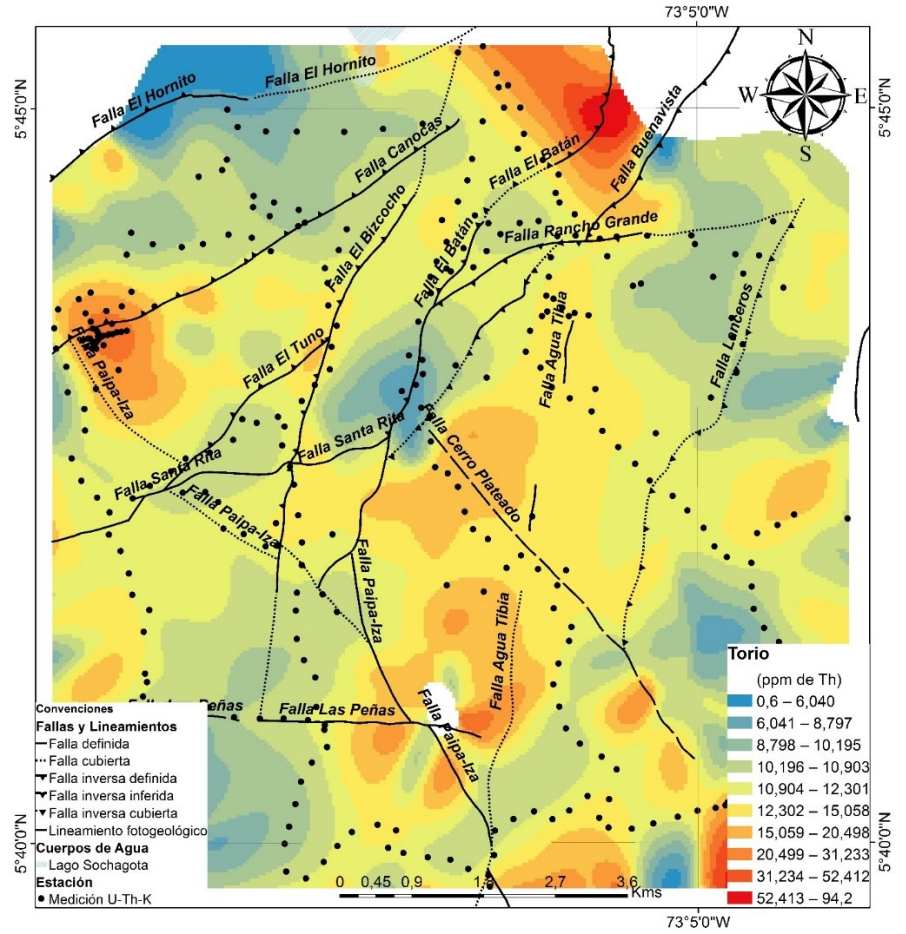
73°5'0"W
5°45'0"N
5°40'0"N
N
W
E
S
Falla El Hornito
Falla Canoas
Falla El Batán
Falla Buenavista
Falla Rancho Grande
Falla El Bizcocho
Falla Agua Tibia
Falla Lenteros
Falla El Tuno
Falla Paipa-Iza
Falla Santa Rita
Falla Cerro Plateado
Falla Las Peñas
Convenciones
Fallas y Lineamientos
Falla definida
Falla cubierta
Falla inversa definida
Falla inversa inferida
Falla inversa cubierta
Lineamiento fotogeológico
Cuerpos de Agua
Lago Sochagota
Estación
Medición U-Th-K
0 0,45 0,9 1,8 2,7 3,6 Kms
Torio
(ppm de Th)
0,6 – 6,040
6,041 – 8,797
8,798 – 10,195
10,196 – 10,903
10,904 – 12,301
12,302 – 15,058
15,059 – 20,498
20,499 – 31,233
31,234 – 52,412
52,413 – 94,2

c)

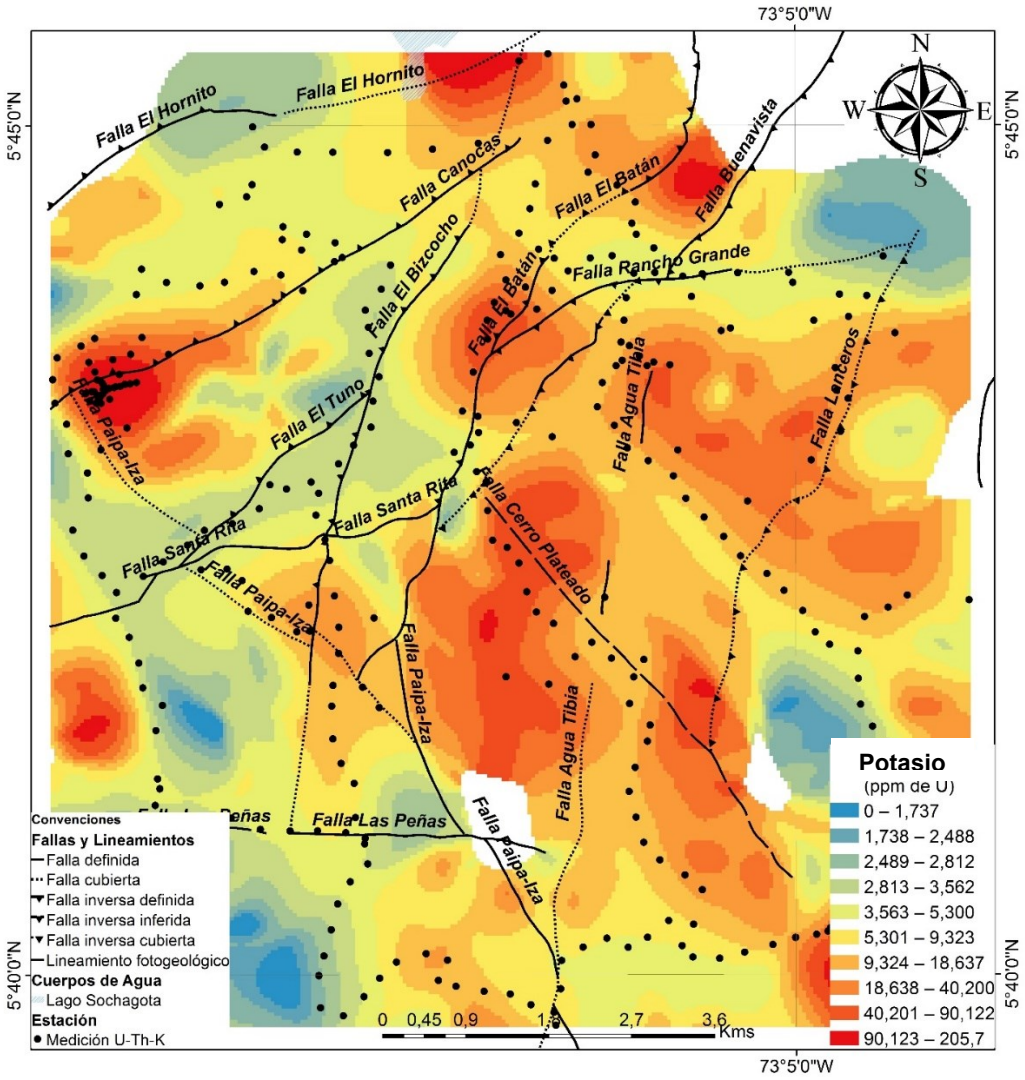

Figure 6: Anomalies maps for a) Uranium (^{38}U), b) Thorium (^{32}Th) and c) Potassium (^{40}K).

The direct comparison of the variables on the same georeferenced linear section allows to analyze and infer the correlations of each temperature anomaly with the referents of the other variables, identifying spatially the points of interest. This spatial analysis starts from the spatialization of the variables of interest (topography, vegetation indices, temperature, radioactive elements, gases, geology, gravity, magnetism, resistivity, among others). Figure 5 shows an example of cross section with the intersection on the same section of variables such as surface temperature, temperature in depth, anomalies of different elements and topography.

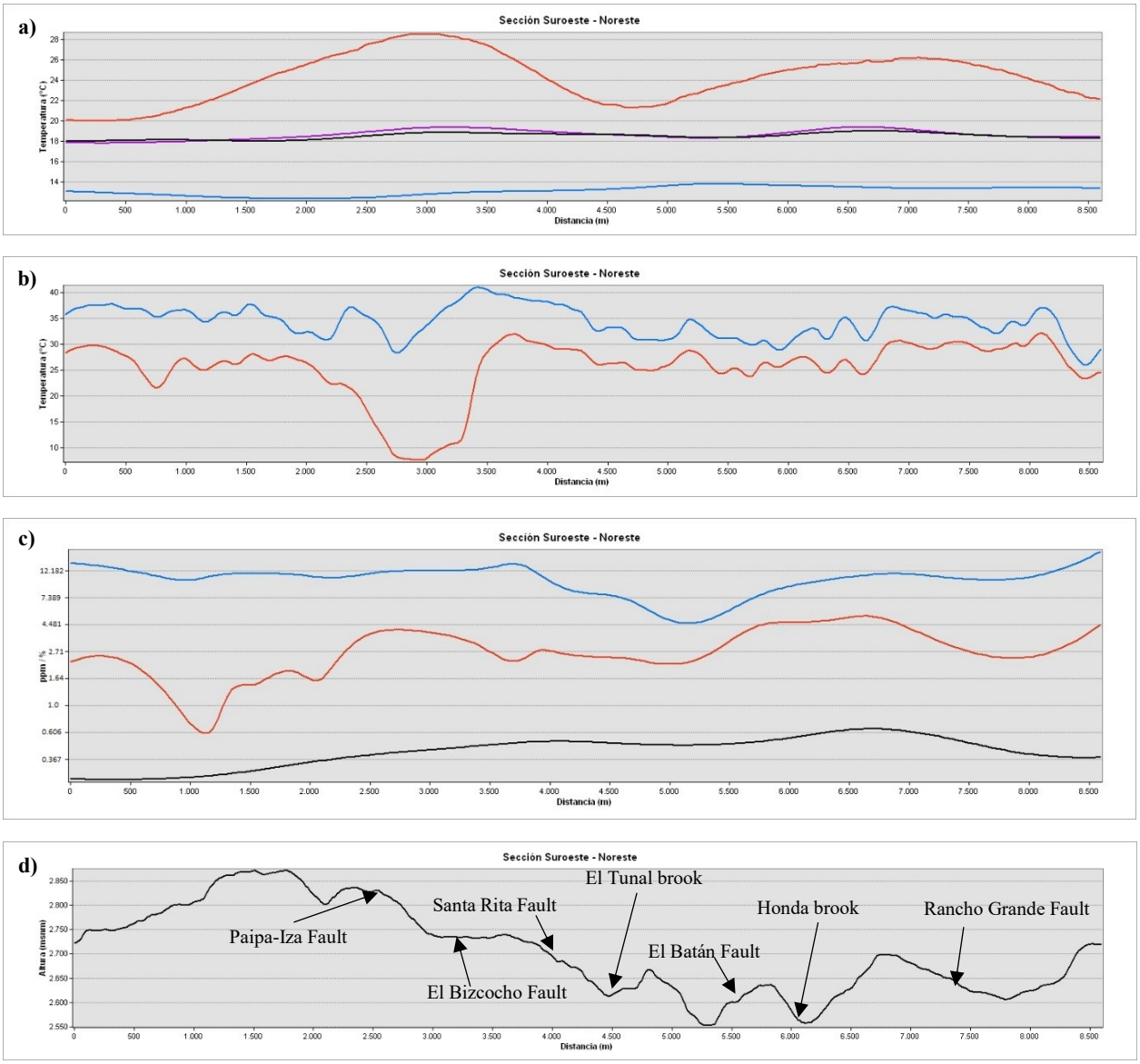

Temperature calculated at 0 cm	Temperature measured at 0 cm	Temperature measured at 20 cm	Temperature measured at 150 cm
Temperature calculated for the day 03/31/2014		Temperature calculated for the day 02/16/2016	
Uranium concentration (ppm)	Thorium concentration (ppm)	Potassium concentration (%)	

Figure 7: Correlation of a) SST, b) Landsat 8 TIRS temperatures, c) U-Th-K anomalies and d) topography in a cross section drawn for the geothermal area of Paipa.

4. DISCUSION AND CONCLUSIONS

The consolidation of the RS as a tool for the generation of surface temperature models is strengthened as a real option for the exploration of geothermal resources in the areas of interest of the Colombian territory. The implementation of these results together with the SST, allow to build a preliminary view of the heat distribution in the geothermal areas in exploration, integrating the values reached at different depths and the influence of geological and geochemical factors together with the topography, granting a first indication of the geothermal structure of the area, allowing to improve the decision making in future studies.

The SST as ground truth, constitute a first perspective of the heat distribution in the exploration geothermal areas. In turn, the remote sensing provides validation of the geothermal structure of the area, through the integration of the NDVI, anomalies of elements such as uranium, thorium and potassium and the estimated temperatures for the various days of study. The influence of topography is an important criterion due to the influence of this variable both for the achievement of field measurements and for the interference of the altitude in the correction factors at the digital levels of the satellite image.

The estimation of the Pearson correlations coefficients greatly constrains (as a good way to reduce the uncertainty) the validation of the results found by means of the RS against the ground truth (SST). This form of validation gives the user a reliable methodology, which allows him to contrast the results achieved through the digital processing of satellite images. These techniques take advantage of a point of control derived from what is observed in the field, adding to the initial inputs that allow the identification of a geothermal area with all its components.

Characterizing temperature anomalies found in the area s of interest present in Colombia, have the potential to reduce costs and constrict the components of a geothermal area in the early exploration stage. In turn, for direct uses, specifically in the installation of heat exchangers for domestic use, they are very useful, since when mapping the anomalies near the surface, a direct relationship is established with the depths where the resource can be exploited in this way.

The processing of images with data in the thermal infrared bands, allows to give a first guideline in the identification of possible temperature anomalies near the surface that do not necessarily depend on a convective heat flow system, thus being able to interpret with a first tool Temperature variations for conductive geothermal systems (such as those present in sedimentary basins). The processing of the thermal band could be enriched by including thermal images of other sensors (e.g., ASTER), which would allow a fusion from different sources to gain in spectral resolution.

REFERENCES

Abouriche, M.: Temperature measurements at the surface and in shallow drillholes, UN Geothermal Training Program, *Technical Report*, Reykjavík, Iceland (1989).

Beardsmore, G.: Towards a shallow Heat Flow probe for mapping thermal anomalies, *Proceedings*, Thirty-Seventh Workshop on Geothermal Reservoir Engineering, Stanford University, Stanford, CA, USA, **37**, (2012), 1-14.

Baddi, M., Guillen, O., Lugo Serrato, O., and Aguilar Garnica, J.: Non-Parametric Correlation and its Application in Scientific Investigations, *International Journal of Good Conscience*, **9**, (2014), 31-40.

Becerra-González, L., Matiz-León, C., Ariza-Ariza, O., Borda-Beltrán, D. and Medina, J.: Application of satellite images and UAV systems for the production of guava in the province of Vélez, Santander, *UD and Geomatics*, **11**, (2016), 46-53.

Coolbaugh, M., Sladek, C., Zehner, R. and Kratt, C.: Shallow Temperature Surveys for Geothermal Exploration in the Great Basin, USA, and Estimation of Shallow Aquifer Heat Loss, *Transactions*, GRC, **38**, (2014), 115-122.

Coolbaugh, M., Sladek, C., Faulds, J., Zehner, R., and Opplieger, G.: Use of rapid temperature measurements at a 2-meter depth to augment deeper temperature gradient drilling, *Proceedings*, Thirty- Second Workshop on Geothermal Reservoir Engineering, Stanford University, Stanford, CA (2007).

Eslava, J.: Altitudinal profile of the average air temperature in Colombia. *Geophysics Colombian*, **1**, (1992), 37-52.

Farr, T., Rosen, P., Caro, E., Crippen, R., Duren, R., Hensley, S., Kobrick, M., Paller, M., Rodriguez, E., Roth, L., Seal, D., Shaffer, S., Shimada, J., Umland, J., Werner, M., Oskin, M., Burbank, D., and Alsdorf, D.: The Shuttle Radar Topography Mission. *Reviews of Geophysics*, **45**, (2007), 1-33.

González, L., Vásquez, L., Muñoz, R., Gomes, H., Parrado, G., and Vargas, S.: Exploration of energy resources. Exploration of Uranium in Paipa, Iza, Pesca, Chivata (Boyacá), *Technical Report*, Ingeominas. Bogotá D.C. (2008).

Kratt, C., Coolbaugh, M., Peppin, B., and Sladek, C.: Identification of a New Blind Geothermal System with Hyperspectral Remote Sensing and Shallow Temperature Measurements at Columbus Salt Marsh, Esmeralda County, Nevada, *Transactions*, Geothermal Resources Council, **33**, (2009), 481-485.

Li, M., Liu, S., Zhou, H., Li, X. and Wang, P.: The Temperature Research of Urban Residential Area with Remote Sensing, *Proceedings*, IEEE International Geoscience and Remote Sensing, **3**, (2005), 1514-1517.

Matiz-León, J.C. Geological conceptual model - geophysical of the geothermal area of Paipa, Boyacá, *Technical Report*, Exploration Group of Geothermal Resources, Colombian Geological Survey – SGC, Bogotá D.C. (2015).

Mermer, A., Yildiz, H., Ünal, E., Aydoğdu, M., Özaydın, A., Dedeoğlu, F., Urla, O., Aydoğmuş, O., Torunlar, H., Tuğaç, M., Avağ, A., Ünal, S., Mutlu, Z.: Monitoring rangeland vegetation through time series satellite images (NDVI) in Central Anatolia Region, *Proceedings*, Fourth International Conference on Agro-Geoinformatics, Istanbul (2015).

Mwawongo, G.: Geothermal mapping temperature measurements, *Technical Report*, Short Course II on Surface Exploration for Geothermal Resources, UNU-GTP and KenGen, Lake Naivasha Kenya (2007).

Norini, G. Gropelli, G., Sulpizio, R., Carrasco- Nunez, G. Davila -Harris, P., Pellicioli, C., Zucca, F. and De Franco, R.: Structural analysis and thermal remote sensing of the Humeros Volcanic Complex: Implications for volcano structure and geothermal exploration, *Journal of Volcanology and Geothermal Research*, **301**, (2015), 221-237.

Olmsted, F., & Ingebritsen, S.: Shallow subsurface temperature surveys in the basin and range province - II. Ground temperatures in the Upsal hogback geothermal area, west - Central Nevada, USA, *Geothermics*, **15**, (1986), 267-275.

Restrepo, L. and González, J.: From Pearson to Spearman, *Colombian Journal of Animal Sciences*, **20**, (2007), 183-192.

Rodríguez, G.: Analysis of the heat distribution in the geothermal area of the Azufral Volcano from surface temperature surveys, *Technical Report*, Exploration Group of Geothermal Resources, Colombian Geological Survey - SGC. Bogotá D.C. (2016).

Rodriguez, G.: Surface Thermal Surveys in the geothermal area of Paipa, Boyacá, *Technical Report*, Exploration Group of Geothermal Resources, Colombian Geological Survey - SGC. Bogotá D.C. (2013).

USGS.: Landsat (L8), Data Users Handbook, *Manual*, Sioux Falls, South Dakota, US Geological Survey, (2016).